

Observations and analysis of polar stratospheric clouds detected by POAM III during the 1999/2000 Northern Hemisphere winter

R. M. Bevilacqua,¹ M. D. Fromm,² J. M. Alfred,² J. S. Hornstein,¹ G. E. Nedoluha,¹ K. W. Hoppel,¹ J. D. Lumpe,² C. E. Randall,³ E. P. Shettle,¹ E. V. Browell,⁴ C. Butler,⁵ A. Dörnbrack,⁶ and A. W. Strawa⁷

Received 7 February 2001; revised 26 June 2001; accepted 6 August 2001; published 4 October 2002.

[1] We present an overview of polar stratospheric cloud (PSC) measurements obtained by POAM III in the 1999/2000 Northern Hemisphere winter. PSCs were observed at POAM latitudes from mid-November to 15 March. PSCs in the early season generally occurred between 17 and 25 km. The central altitude of the PSC observations, roughly 21 km, is unchanged between November and late January. PSCs were not observed between 7 and 27 February. When they reappeared, they formed at distinctly lower altitudes, centered roughly at 16 km. We also present both qualitative and quantitative comparisons with airborne lidar and in situ balloon measurements of PSCs obtained over the Norwegian Sea and Scandinavia over the 25–27 January time period. We find that the large-scale PSC altitude features and morphology are well reproduced in the POAM measurements. Finally, we use PSC occurrence probabilities, analyzed as a function of ambient temperature relative to the NAT saturation point, to infer irreversible denitrification. This denitrification is observed to maximize in late February at levels of at least 75% in the 19–21 km region, with similar values in the 16–18 km region. No denitrification was inferred above 21 km or below 16 km. *INDEX TERMS*: 0305

Atmospheric Composition and Structure: Aerosols and particles (0345, 4801); 0340 Atmospheric Composition and Structure: Middle atmosphere—composition and chemistry; *KEYWORDS*: polar stratospheric clouds (PSCs), polar stratospheric temperatures, vortex phenomena, denitrification

Citation: Bevilacqua, R. M., et al., Observations and analysis of polar stratospheric clouds detected by POAM III during the 1999/2000 Northern Hemisphere winter, *J. Geophys. Res.*, 107(D20), 8281, doi:10.1029/2001JD000477, 2002.

1. Introduction

[2] The combined SAGE III Ozone Loss and Validation Experiment (SOLVE) and Third European Stratospheric Experiment on Ozone II (THESEO II) campaign (hereafter referred to as the SOLVE/THESEO 2000 campaign) was a multiplatform measurement and modeling mission designed to investigate processes responsible for ozone loss at high northern latitudes. Because of their importance in polar ozone photochemistry [e.g., Solomon, 1999], polar stratospheric clouds (PSCs) were an important science focus of the SOLVE/THESEO 2000 campaign.

[3] The Naval Research Laboratory's Polar Ozone and Aerosol Measurement (POAM III) instrument is well suited for studying polar ozone processes because it provides continuous measurements over the polar regions of both hemispheres. POAM III was fully operational during the SOLVE/THESEO 2000 campaign. An important POAM III science objective is the measurement of PSCs. The SOLVE/THESEO 2000 mission presented an excellent opportunity to examine the spatially and temporally extended PSC measurements from POAM III in the context of the more localized, high spatial resolution balloon and airborne measurements made during the campaign. An important strength of satellite measurements such as POAM is that they typically provide comprehensive multiyear data sets. While it is not feasible to support a mission of the size and scope of the SOLVE/THESEO 2000 campaign each year, presumably there will be satellite measurements available each year. Thus it is important to use the SOLVE/THESEO 2000 mission to evaluate deficiencies and strengths in the ability of satellite measurements to obtain the required PSC information to evaluate polar ozone loss. Furthermore, the global view provided by the satellite measurements provides a context from which the more localized SOLVE/THESEO 2000 measurements can be viewed.

[4] In this paper we give an overview of the POAM PSC observations obtained during the 1999/2000 winter. First,

¹Naval Research Laboratory, Washington, D. C., USA.

²Computational Physics, Inc., Springfield, Virginia, USA.

³Laboratory for Atmospheric and Space Physics, University of Colorado, Boulder, Colorado, USA.

⁴Lidar Application Group, NASA Langley Research Center, Hampton, Virginia, USA.

⁵SAIC, Lidar Application Group, NASA Langley Research Center, Hampton, Virginia, USA.

⁶DLR Oberpfaffenhofen, Institut für Physik der Atmosphäre, Wessling, Germany.

⁷NASA Ames Research Center, Moffett Field, California, USA.

we present quantitative comparisons of POAM PSC measurements with coincident measurements obtained with the NASA DC-8 Differential Absorption Lidar (DIAL) instrument, and the DLR-Falcon Ozone Lidar Experiment (OLEX) instrument on 25 and 26 January 2000 over the Norwegian Sea. We also present more qualitative comparisons with near coincident measurements obtained over Scandinavia during the same time period. We then give an overview of the POAM PSC observations obtained during the 1999/2000 winter, and contrast these observations with those obtained in earlier Northern Hemisphere winters. Finally, we correlate PSC occurrence with the region of the atmosphere saturated with respect to nitric acid trihydrate (NAT) PSCs. We examine in detail the PSC observation probability as a function of ambient temperature relative to the NAT saturation temperature (T_{NAT}), and the evolution of these probabilities over the season. We conclude that this evolution is most likely driven by the irreversible denitrification, which was well documented during this winter [Popp *et al.*, 2001]. We analyze variations in the POAM PSC observation probabilities to make quantitative estimates of the magnitude of this denitrification, and compare these to other observations.

2. POAM Instrument and PSC Measurements

[5] POAM III is a satellite-based nine-channel, visible/near-infrared photometer for making measurements of ozone, aerosol extinction, water vapor, and nitrogen dioxide in the polar stratosphere using the solar occultation technique [Lucke *et al.*, 1999]. POAM III was launched in March 1998, is currently operational, and was fully operational during the SOLVE/THESEO 2000 campaign. POAM III is the successor to, and improved version of, the POAM II instrument [Glaccum *et al.*, 1996] which operated from October, 1993 to November 1996. (For brevity, throughout this paper, unless otherwise noted, “POAM” will refer to POAM III).

[6] Like NASA’s Halogen Occultation Experiment (HALOE) [Russell *et al.*, 1993] and Stratospheric Aerosol and Gas Experiment (SAGE II) [Mauldin *et al.*, 1985] solar occultation instruments, POAM makes 14–15 measurements per day in each hemisphere around a circle of latitude, with a longitude spacing of about 25° . The measurement latitude slowly varies over the year. Because POAM is in a 98.7° Sun synchronous orbit (rather than the 57° inclination orbits of HALOE and SAGE II) the POAM measurements are confined to high latitudes in both hemispheres. In the Northern Hemisphere the annual measurement range is 55°N to 73°N . The measurement coverage exhibits nearly exact annual periodicity. (A graphical representation of the POAM Northern Hemisphere measurement coverage is shown by Lumpe *et al.* [2002a, Figure 1]). During the SOLVE/THESEO 2000 campaign the POAM Northern Hemisphere measurement latitude varied from about 64° in early December, increasing monotonically to a maximum of 67.7° in early March. Kiruna, Sweden (the SOLVE/THESEO 2000 campaign home base) is located at about 68°N latitude. Thus the POAM measurement sampling was well suited to supporting the SOLVE/THESEO 2000 campaign.

[7] The POAM PSC data reported here were obtained by adapting to POAM III the POAM II PSC detection algo-

rithm given by Fromm *et al.* [1997] and revised by Fromm *et al.* [1999]. This technique uses enhancements in the POAM 1018 nm aerosol extinction profiles to denote PSC presence. Briefly, a clear air aerosol extinction profile (average and standard deviation) is computed for both inside and outside the vortex. Each POAM profile, at each altitude, is first delineated with respect to the polar vortex and compared to the appropriate (inside or outside the vortex) clear-air value. Any retrieved aerosol extinction value which is more than 2.7 standard deviations higher than the appropriate clear-air average value, and which occurs at a temperature lower than a screen value (which varies linearly from 197.5 K at 25 km to 203.5 K at 13 km), is assumed to be a PSC. The PSC search altitude region is 13 to 25 km, but is restricted to altitudes at least 3 km above the tropopause (defined here using a potential vorticity value of $2 \times 10^{-6} \text{ K m}^2 \text{ kg}^{-1} \text{ s}^{-1}$ (2PVU) [Appenzeller *et al.*, 1996]) to ensure against contamination by high cirrus. The POAM II PSC detection algorithm has been validated by comparison with ground-based lidar measurements by Fromm *et al.* [1997]. That paper also presents an overview of POAM II PSC observations in the 1994 through 1996 Antarctic winters. Fromm *et al.* [1999] give the POAM II Northern Hemisphere PSC climatology (1993/1994 through 1995/1996).

[8] In addition to PSC detection, the POAM measurements have been used to infer information about PSC composition. First, the POAM minimum tracking altitude has been used as a proxy indicator of type II (water ice) PSCs. The details and justification for this procedure are given by Fromm *et al.* [1997, 1999]. Briefly, by an analysis of the POAM instrument model and an ensemble of PSC microphysical models, we have shown that only ice clouds are likely to become sufficiently opaque to cause POAM event termination above 16 km. Thus events which terminate above this altitude suggest the presence of an ice cloud from 0 to 3 km below the termination altitude [Fromm *et al.*, 1999]. Also, Strawa *et al.* [2002] use the relation between aerosol extinction color ratio (1018 nm extinction/603 nm extinction) and 1018 nm aerosol extinction in PSCs to distinguish crystalline (type Ia) from liquid (type Ib) PSCs.

[9] The estimated random errors in the POAM 1018 nm aerosol extinction retrievals, on which the POAM PSC detection algorithm is based, are less than 15% below 23 km, increasing to near 40% at 30 km [Lumpe *et al.*, 2002b]. The aerosol retrievals have been validated, by comparison to SAGE II and HALOE measurements, by Randall *et al.* [2001]. The vertical resolution of the POAM 1018 nm aerosol extinction retrievals is a function of altitude, and varies from about 1.9 km at 13 km, to a minimum of about 1.3 km at 20 km, and increases above 20 km to about 2.0 km at 25 km (Lumpe *et al.*, submitted manuscript, 2001). The horizontal resolution (in each 1 km shell) is about 250 km along the line of sight, and about 30 km perpendicular to the line of sight [Lucke *et al.*, 1999]. Because POAM is a solar occultation instrument, the measurement line of sight is always oriented toward the Sun.

3. POAM Measurement Sampling

3.1. Sampling With Respect to the Vortex

[10] Figure 1 shows the equivalent latitude, on the 500 and 650 K potential temperature surfaces (approximately

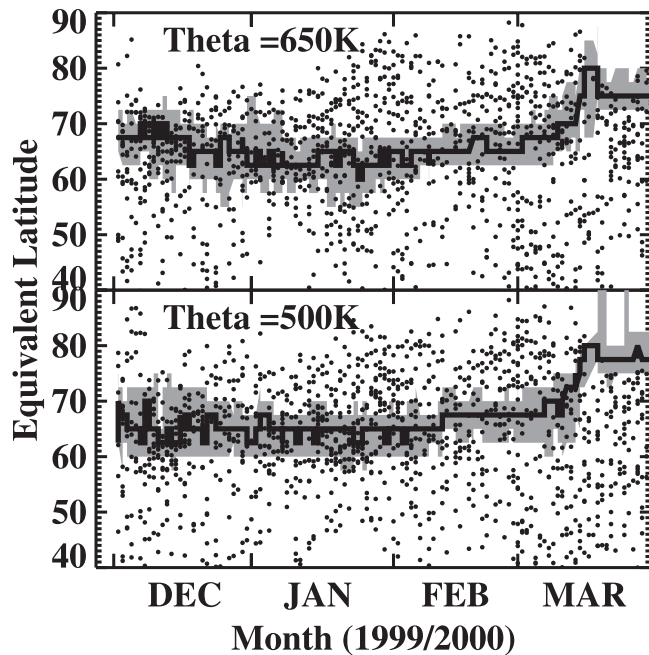


Figure 1. Equivalent latitude of each POAM measurement point at the indicated potential temperature levels for the 1999/2000 Northern Hemisphere winter. The solid lines denote the center of the vortex boundary region, and the shaded region bounds the inner and outer edges as determined using the *Nash et al.* [1996] delineation technique and the UKMO analysis.

20 and 25 km), of each POAM measurement obtained during the SOLVE/THESEO 2000 campaign. Equivalent latitude is a vortex centered coordinate system based on the Ertel's potential vorticity (E_{pv}) field, defined as the latitude that would enclose the same area between it and the pole as a given E_{pv} contour [Butchart and Remsberg, 1986]. The E_{pv} fields needed to compute equivalent latitude were obtained from the daily (valid at 1200 Greenwich Mean Time (GMT) each day) United Kingdom Meteorological Office (UKMO) [Swinbank and O'Neill, 1994] analysis interpolated to the time and location of each POAM measurement. Also shown are the equivalent latitudes of the center, and poleward and equatorward edges of the vortex boundary region at the indicated potential temperature levels. The E_{pv} values of the vortex boundaries were computed using E_{pv} and wind fields from the UKMO analysis, and the objective vortex discrimination algorithm given by *Nash et al.* [1996]. In general, POAM samples out of the vortex, in the vortex boundary region, and inside the vortex on a daily basis throughout the winter. However, through mid-January POAM did not sample at the very center of the vortex, especially at 650 K. This was because the vortex tended to be more centered on the pole in the early part of the winter than is typically the case in the Arctic [see *Manney and Sabutis*, 2000, and references therein]. Thus even POAM's inside vortex measurements at this time were not at the vortex core (this point is discussed further below). However, from about the beginning of February through mid-March, POAM sampled to the vortex center on a routine basis.

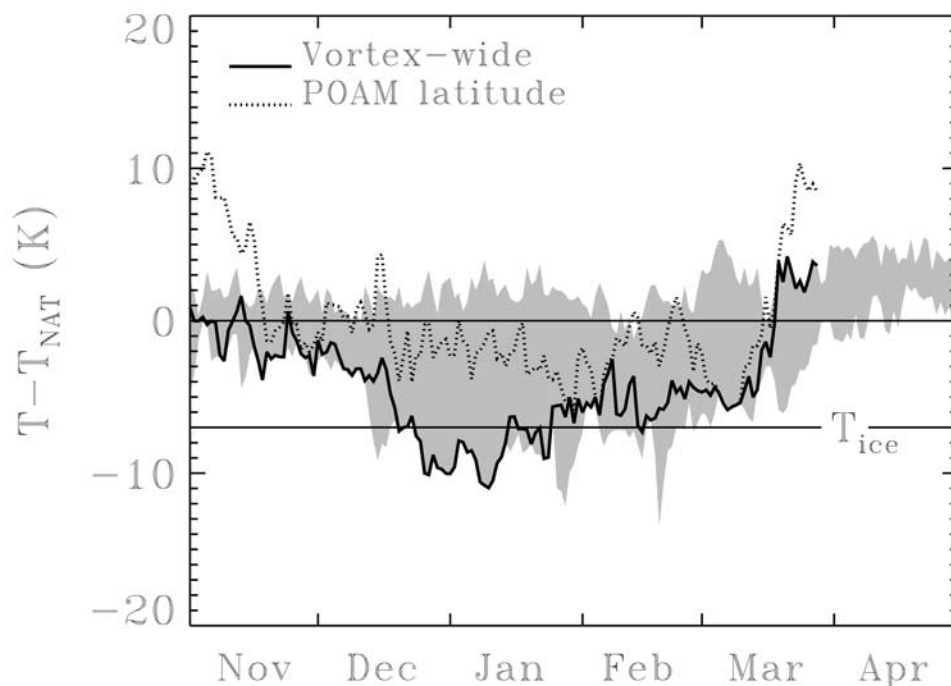


Figure 2. Time series of $T - T_{\text{NAT}}$ over the 10–150 hPa range for the 1999/2000 winter for: vortex-wide minima (solid line), and POAM measurement latitude minima (dashed line). The shaded region gives the climatological range of the vortex-wide minima for the 1994 to 2000 winters. Temperatures and pressures were obtained from the UKMO analysis, and T_{NAT} values were obtained using the expression given by *Hanson and Mauersberger* [1988] with an assumed H_2O and HNO_3 mixing ratio of 5 and 10 ppbv, respectively. T_{ice} values were obtained using the formulation by *Jansco et al.* [1970].

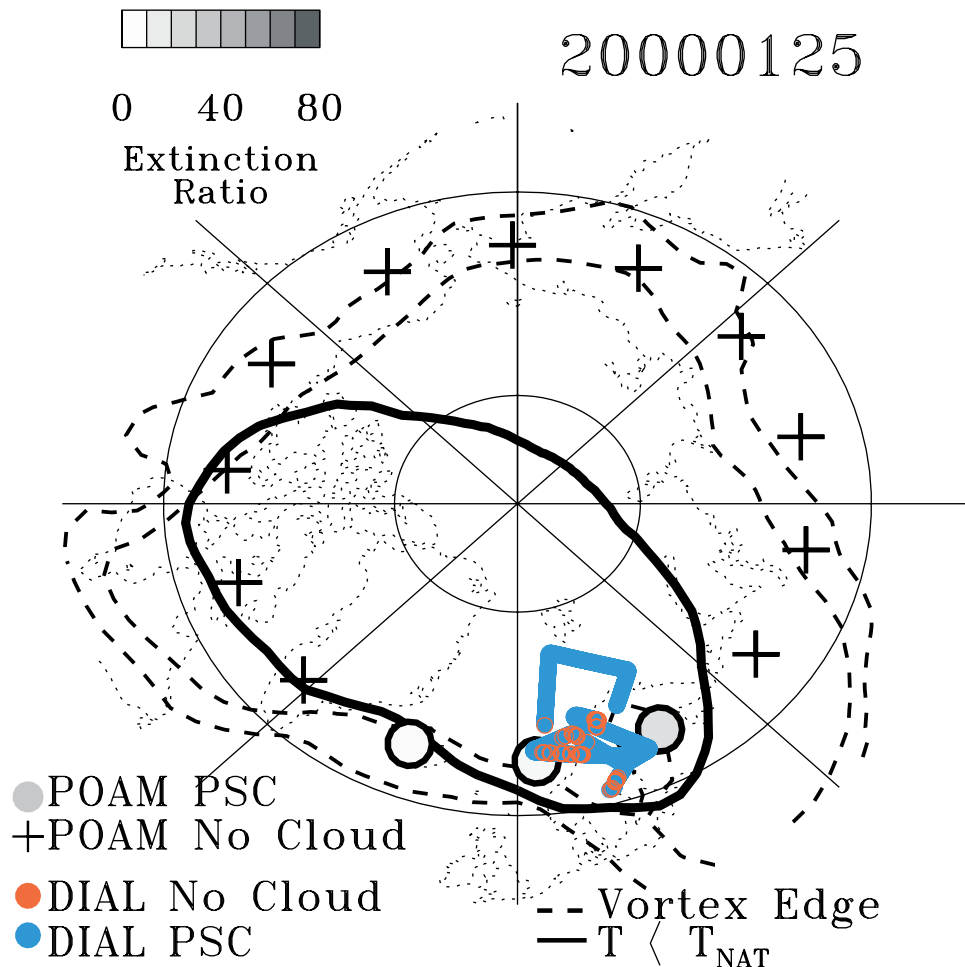


Figure 3a. Polar orthographic projection, centered on the North Pole, showing the POAM 25 January 2000 measurement locations. PSCs are indicated by the large circles, and the gray shading gives the peak aerosol extinction ratio in the cloud (defined as the ratio of aerosol to Rayleigh extinction). Plus signs indicate POAM measurements in which no PSCs were observed. Also indicated is the Nash polar vortex edge region (outer and middle edge of the vortex) (dashed contour pair), and the $T - T_{\text{NAT}} = 0$ K contour (solid line) evaluated on the 500 K isentropic surface. The blue and red filled circles show the NASA DC-8 flight track. Blue symbols denote portions of the flight track in which the DIAL instrument observed a PSC, and red symbols denote cloud-free portion of the flight track.

3.2. Sampling With Respect to Temperature

[11] In Figure 2, we plot daily minimum temperatures for the 1999/2000 winter, with respect to the NAT saturation point (i.e., $T - T_{\text{NAT}}$), both at the POAM measurement latitude and for the entire vortex (defined here as the region inside the *Nash et al.* [1996] outer edge). The shaded region denotes the range of vortex-wide minimum temperatures over the 1994 to 2000 period, and is shown for context. For this analysis we calculate a daily temperature minimum (T_{min}) using the UKMO gridded temperature field. T_{min} takes into account pressure levels from 150 to 10 hPa. For the T_{NAT} computation we use the formulation given in *Hanson and Mauersberger* [1988] assuming a constant water vapor and nitric acid (HNO_3) mixing ratio of 5 ppmv and 10 ppbv respectively. (A constant water vapor mixing ratio was used for this plot instead of POAM water vapor because it is a multiyear climatology during which POAM water vapor is not generally available.) The water vapor

frost point (T_{ice}) was obtained using the formulation given by *Jansco et al.* [1970].

[12] The time period considered in Figure 2 includes three Northern Hemisphere winters in which the stratosphere was colder than average (1994/1995, 1995/1996, and 1996/1997), the relatively warm 1997/1998 winter [*Pawson and Naujokat*, 1999], and the 1998/1999 winter which was also warm, and featured two major stratospheric warmings [*Manney et al.*, 1999]. *Manney and Sabutis* [2000], in an analysis of the temperature evolution during the 1999/2000 Arctic winter, concluded that the winter was unusually cold, and that the area of the vortex with temperatures near the PSC threshold in December and January was larger than that obtained in any previously observed winter. Consistent with this analysis, Figure 2 shows that, over most of the winter, the 1999/2000 temperature values define the minimum of the total range obtained during the 1994–2000 period. Temperatures decreased below the NAT condensation point in

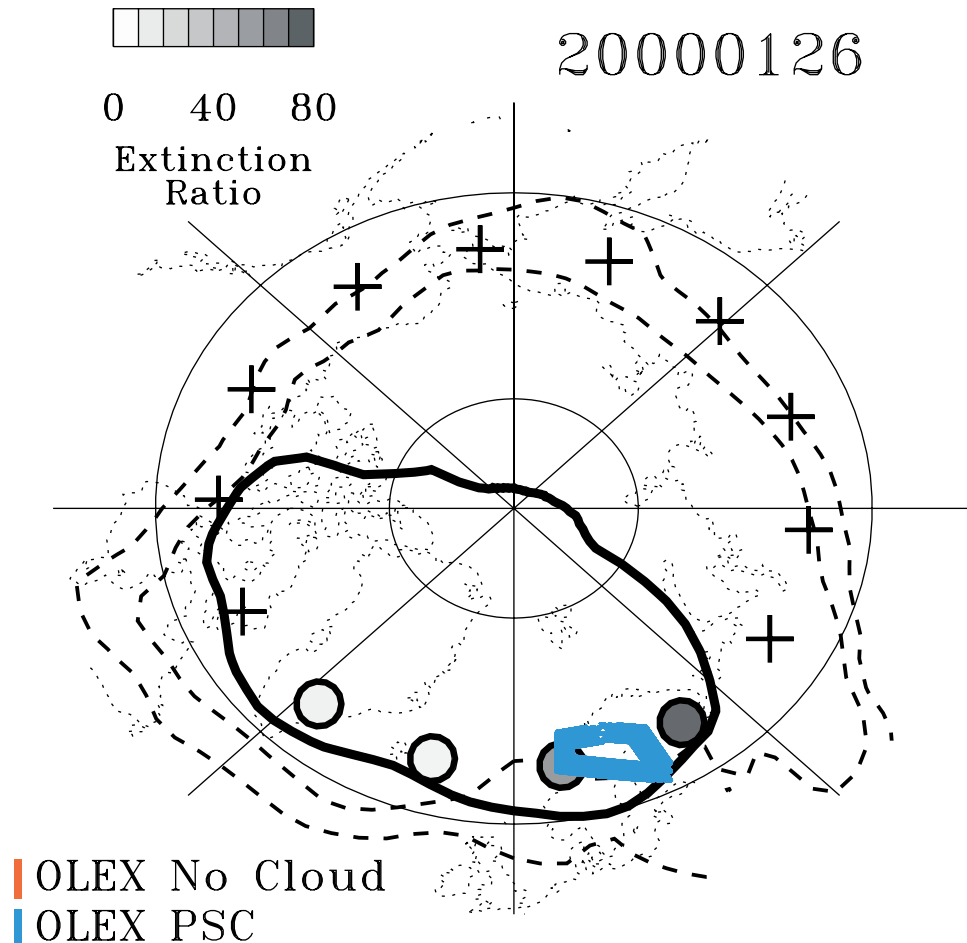


Figure 3b. Same as Figure 3a for 26 January 2000. In this case the DLR Falcon flight track is shown, and the OLEX measurements are indicated.

November, and remained below this value until mid-March. However, with regard to the POAM sampling, the dashed line shows that from the beginning of the winter through late February, POAM did not sample the coldest vortex air (except for short periods in early December, late January, and early February). This is because the vortex and the coldest air tended to be centered near the pole. However, in March the cold pool shifted off the pole to a position centered over northern Russia, close to the POAM measurement latitude, allowing POAM to sample the coldest stratospheric air.

4. POAM, Lidar, and In Situ Balloon PSC Comparisons: 25–27 January 2000

[13] In this Section we evaluate the POAM PSC measurements by comparison with the higher resolution airplane and balloon-borne measurements obtained during the SOLVE/THESEO 2000 campaign. For these comparisons we use the 25–27 January 2000 time period. This period was selected because PSCs were well documented over Scandinavia at latitudes close to the POAM measurement by other measurements made as part of the SOLVE/THESEO 2000 campaign. These include airborne lidar measurements, made aboard both the NASA DC-8 and the DLR

Falcon, which have documented the role of inertial gravity waves in the production of PSCs in the lee of the Scandinavian mountains [Dörnbrack *et al.*, 2002]. In addition, on 25 January in situ PSC observations were made from a balloon-borne payload launched from Kiruna [Voigt *et al.*, 2000].

[14] In Figures 3a–3c we show the locations of the POAM measurements obtained on 25 through 27 January and indicate where PSCs were observed. Also plotted on the figures are the middle and equatorward edge of the polar vortex, and the $T = T_{\text{NAT}}$ temperature contour on the 500 K potential temperature surface, both calculated using the UKMO analysis valid at 1200 GMT for each day as described in section 3. We note that the $T = T_{\text{ice}}$ contour at 500 K would also have been plotted, but temperatures that low were not obtained (although temperatures less than T_{ice} were found on 24 January east of Greenland). The meteorological conditions during this period are described by Dörnbrack *et al.* [2002]. Figure 4 shows that POAM observed PSCs in the vicinity of the Greenwich meridian on all three days. On 25 January POAM observed a PSC on three consecutive orbits (each occurring roughly 100 minutes apart) from 29° to 338°E , with the strongest PSC (in terms of extinction enhancement) at 29°E . On this day the cold pool (core of the coldest air) was oriented very

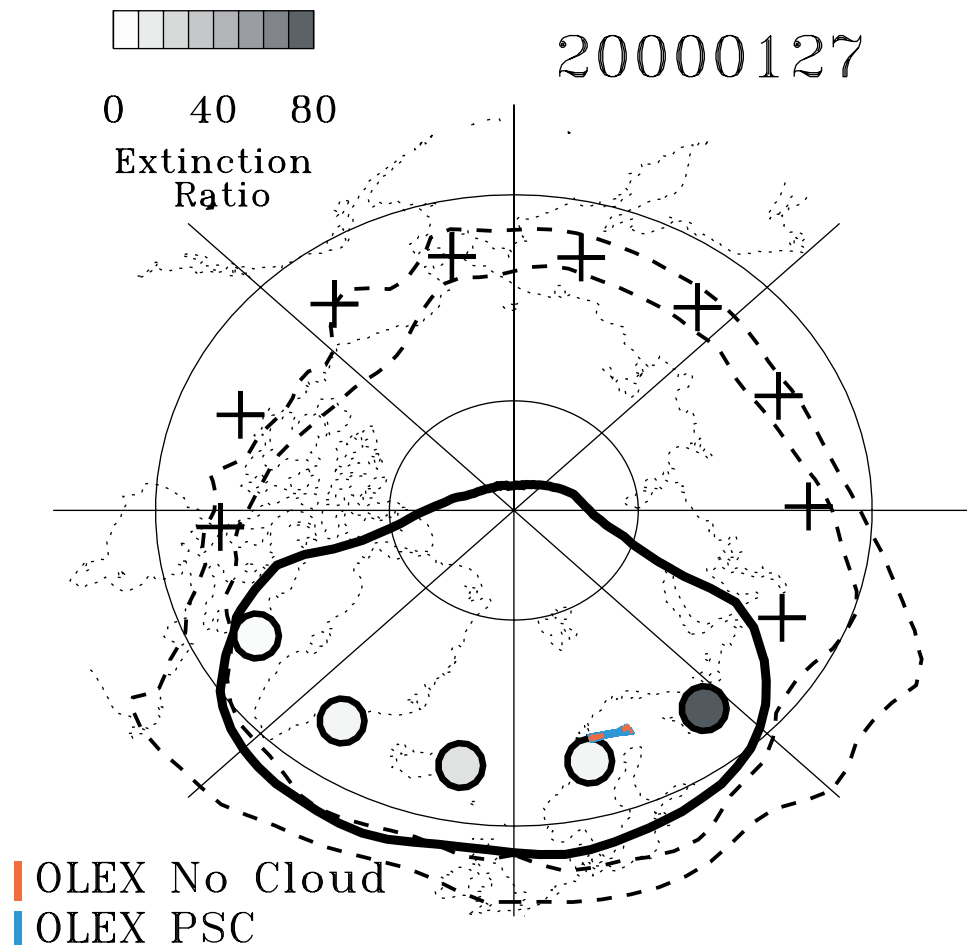


Figure 3c. Same as Figure 3a for 27 January 2000. Again the DLR flight track and the OLEX measurements are indicated.

close to the vortex edge, and all three POAM PSC observations straddled the vortex edge. The measurement at the Greenwich meridian was made at temperatures approaching the water ice frost point, but we infer that this PSC was not type II (water ice) because the measurement altitude cutoff criterion, given by *Fromm et al.* [1999] and discussed above, was not met. Minimum vortex temperatures were somewhat warmer on 26 and 27 January. PSCs were observed over Scandinavia on both of these days, but west to Greenland as well. Although not shown, on all three days POAM sampled very near the cold pool.

[15] Figure 3a shows the NASA DC-8 flight track, and Figures 3b and 3c the DLR Falcon flight tracks for the indicated days. Plotted along the flight tracks of these two figures are indicators of PSC and PSC-free conditions obtained from the OLEX (DLR Falcon) and DIAL (NASA DC-8) measurements using the backscatter PSC criterion given by *Dörnbrack et al.* [2002]. These show that PSCs were nearly ubiquitous over the DC-8 flight track on 25 January and the DLR Falcon flight track on 27 January and entirely so over the DLR Falcon flight track on 26 January. The OLEX measurements obtained on 26 January shown by *Dörnbrack et al.* [2002, Figure 7], indicate a relatively homogeneous, large-scale PSC layer over the Norwegian Sea, west (i.e., upwind) of the Scandinavian

coast, and a PSC complex with large spatial variability east of the mountains. We contend that the lidar and POAM measurements suggest that the lee wave-induced PSCs observed by the DLR Falcon and NASA DC-8 during this time period [*Dörnbrack et al.*, 2002] were actually modulations and enhancements of much larger scale PSC coverage.

4.1. Comparisons Over the Norwegian Sea

[16] In order to make quantitative comparisons between the lidar and POAM PSC observations we adopt measurement coincidence criteria of $\pm 1^\circ$ latitude, $\pm 2^\circ$ longitude, and ± 1 hour in time. These are the same measurement coincidence criteria employed in the POAM ozone comparisons obtained during the SOLVE/THESEO 2000 campaign presented by *Lumpe et al.* [2002a]. With these criteria, a POAM measurement coincidence was obtained with the DIAL instrument on 25 January and the OLEX instrument on 26 January both over the Norwegian Sea. Direct comparisons between lidar backscatter and POAM extinction measurements are beyond the scope of this paper. This is because their interpretation is complicated by the uncertainty in the extinction to backscatter ratio resulting from its large dependence on the aerosol size distribution, composition, and particle shape. Instead, we compare PSC altitudes

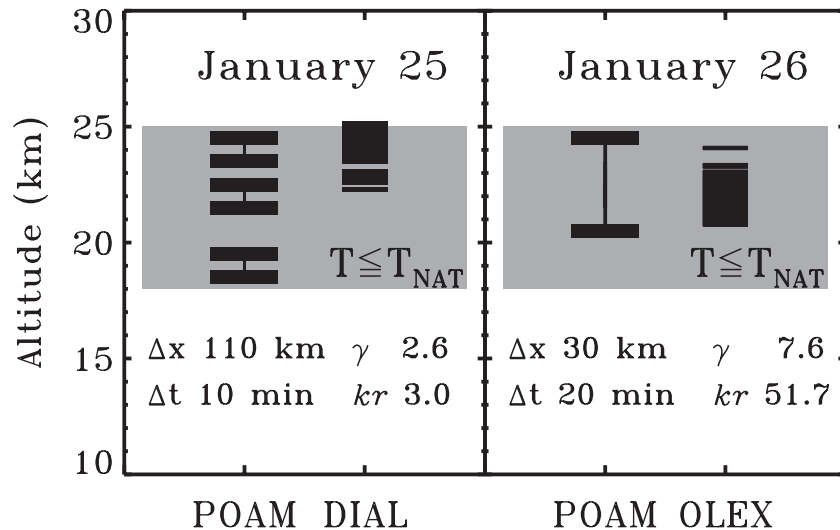


Figure 4. PSC altitude regions for the 25 January POAM/DIAL coincidence (left) and the 26 January POAM/OLEX measurement coincidence (right). The POAM measurement for the 26 January (25 January) coincidences were obtained at 1419 GMT at 65.64°N, 9.37°E (14:39 GMT at 65.55°N, 3.75°E). Each POAM altitude in which a PSC was detected is denoted by a vertical bar with a range of ± 0.5 km centered on the retrieved PSC altitude (the POAM retrievals are done on a 1 km grid centered at integer altitudes). In both cases, the lidar PSC altitudes were obtained by averaging all the lidar data obtained within the adopted measurement coincidence criteria of $\pm 1^\circ$ latitude, $\pm 2^\circ$ longitude, and ± 1 hour in time, and plotting the altitudes in which the average backscatter ratios exceed the PSC threshold value. The vertical resolution of the lidar measurements is about 30 m. The differences in distance and time between the lidar and POAM measurements at the coincidence point are designated by Δx and Δt , respectively. Finally, γ denotes the peak lidar backscatter ration and kr the peak POAM extinction ratio for the measurements.

inferred from the POAM extinction measurements and PSC detection algorithm to PSC altitudes obtained from the lidar backscatter measurements.

[17] In Figure 4 we compare the POAM and lidar PSC altitudes for the two measurement coincidences. In order to determine the lidar PSC altitudes we first constructed an average backscatter ratio profile encompassing all data which fell within the adopted measurement coincidence criteria given above. Figure 4 designates all altitudes in the average profile with backscatter ratios greater than the PSC threshold value. For POAM, we represent all altitudes in which a PSC was detected as a ± 0.5 km vertical bar, centered on the PSC altitudes, because the POAM aerosol extinction retrieval algorithm uses 1 km averaging, centered on each integer kilometer. For both measurement coincidences we also show the region of the atmosphere with temperatures below T_{NAT} , obtained using the UKMO analysis interpolated to the time and location of the POAM measurements as described in section 3.

[18] The POAM/OLEX coincidence obtained on 26 January was by far the closest measurement coincidence. The closest approach in distance and in time for this pair of observations is approximately 29 km and 20 minutes. Furthermore, at this coincidence point, which is very near point C of the DLR Falcon flight as designated by Dörnbrack *et al.* [2002, Figures 6 and 7], PSCs exhibited very little spatial variability. Also, the DLR Falcon flight path between points B and C of the flight was oriented approximately along the POAM line of sight. The POAM observation at this coincidence shows a PSC extending from 21

to 24 km, with peak extinction at 21 km. In the OLEX observation, PSC backscatter enhancements extend from about 20.5 to 23.3 km, with a second, very narrow layer centered at 24 km. This is in excellent agreement with the POAM PSC measurement. In both the POAM and OLEX measurements, PSCs were observed within the region of the atmosphere saturated with respect to NAT. Also, the OLEX observation indicates that the PSCs observed during the POAM coincidence were predominantly composed of liquid particles (type Ib) [Dörnbrack *et al.*, 2002]. The analysis of the POAM PSC measurements by Strawa *et al.* [2002] also suggests that this PSC was predominantly type 1b.

[19] The POAM/DIAL coincidence on 25 January was obtained at the far western edge of the NASA DC-8 east to west transit made during this flight near local sunset. This coincidence was also used in the POAM/UV DIAL ozone comparisons given by Lumpe *et al.* [2002a]. This is not as favorable a measurement coincidence as the POAM/OLEX coincidence discussed above because it is not as close spatially (closest approach is about 110 km compared to 29 km for the OLEX/POAM coincidence), and the aerosol and cloud features exhibit much larger spatial variability than that found on 26 January. To illustrate the inhomogeneity present during the POAM/DIAL coincidence on 25 January, in Figure 5 we show a contour plot of the DIAL backscatter for the east/west transit of the DC-8 flight close to the POAM measurement. The portion of the flight within the coincidence criteria is also shown. On the westbound leg there appears to be a fairly sharp edge to the PSCs at about 5°E, whereas on the return eastbound leg of the flight, just

scatter and POAM extinction threshold value for PSC presence becomes somewhat arbitrary.

[22] Figure 4 also gives the peak aerosol extinction ratio and the peak backscatter ratio for the measurement coincidences. As discussed above, these values cannot be compared directly because of the large uncertainty in the extinction to backscatter ratio. However, it is interesting to note that both POAM and the lidar measurements suggest that the PSCs over the Norwegian Sea on 26 January had much greater optical thickness than those observed on 25 January. This is particularly intriguing because the UKMO temperature profile interpolated to the time and location of the POAM measurements on 25 and 26 January are virtually identical. Many studies [e.g., *Larsen et al.*, 1996, 1997] have shown that temperature history, as well as local temperature, is important in determining PSC physical properties. Thus we speculate that the PSCs observed on those days had different temperature histories.

4.2. Comparisons Over Scandinavia

[23] Although not within the prescribed measurement coincidence criteria, POAM made measurements on 25–27 January over Scandinavia which were in the vicinity of OLEX and DIAL measurements made on those days. In addition, on 25 January a balloon-borne PSC payload was launched from Kiruna [*Voigt et al.*, 2000]. In the following we discuss qualitative comparisons between POAM and the other PSC measurements made over Scandinavia during this period. However, these comparisons must be viewed with caution since, in all cases, closest coincidences were obtained in the lee of the Scandinavian mountains during a period of intense gravity wave activity [*Dörnbrack et al.*, 2002].

[24] Figure 6 shows POAM aerosol extinction ratio profiles obtained in the vicinity of Scandinavia during the 25–27 January time period. OLEX, DIAL, and the balloon-borne PSC measurements were made on 25 January. All three of these measurements were made several degrees to the west of the closest POAM measurement, which occurred at 29.1°E. The balloon-borne measurement was made nearly midway (in time) between the POAM observation on 25 January, and that made on the following day at 34.7°E, while the two airborne lidar measurements were made much closer in time to the 25 January observation. Figure 6 shows that POAM observed a PSC on 25 January extending from 19 to 23 km, and a much smaller PSC layer centered at 17 km. The OLEX measurements in this vicinity show a PSC layer from 19.5 to 23 km, and the DIAL from 19.5 to 22 km [*Dörnbrack et al.*, 2002]. The balloon-borne PSC payload, the altitude of which was guided within saturated air, made PSC measurements between 20.8 and 22 km [*Voigt et al.*, 2000]. Thus the altitude range of the upper PSC layer seen in the 25 January POAM measurement is consistent with the other measurements. There is no indication in the other measurements of the small PSC layer seen at 17 km. However, conditions were quite variable during this period. For example, Figure 6 also shows that the POAM measurement obtained at nearly the same location (5° further east) 24 hours later has a PSC at 21 km, in good agreement with the other measurements, and no evidence of the small layer seen the day before at 17 km.

[25] The OLEX measurements identified the PSC observed on 25 January as a NAT cloud [*Dörnbrack et*

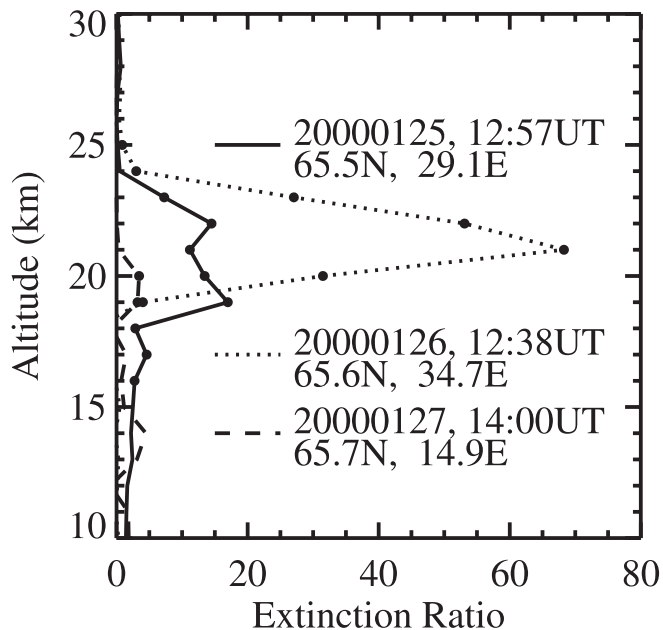


Figure 6. POAM aerosol extinction ratio profiles obtained over Scandinavia at the indicated times and locations. These profiles were obtained in near coincidence with other SOLVE/THESEO 2000 PSC measurements. Dots on the lines indicate where PSC extinctions occurred.

al., 2002]. Mass spectrometer measurements on board the balloon-borne PSC payload also identified the PSCs observed in closest coincidence to the POAM measurement as NAT [*Voigt et al.*, 2000]. In fact, the balloon-borne observation is significant because it was the first direct measurement of NAT particles in a PSC. The POAM PSC discrimination analysis by *Strawa et al.* [2002] indicates that the PSC observed by POAM at this location was a NAT, in agreement with the other measurements.

[26] On 27 January only OLEX and POAM measurements were made. The OLEX measurements suggest that PSC activity was much reduced over Scandinavia compared to that observed on the two previous days as gravity wave activity subsided [*Dörnbrack et al.*, 2002]. Figure 6 shows that the POAM measurement in closest coincidence to the OLEX measurements also indicates a much smaller PSC compared to the 25 and 26 January observations. The POAM observation on 27 January shows a small PSC layer centered at 20 km, while the OLEX measurements show a complex, multilevel cloud structure with PSCs as high as about 25.5 km, and as low as 16 km [*Dörnbrack et al.*, 2002]. Although the POAM measurement does capture the reduced level of PSC activity on 27 January compared to 25 and 26 January over Scandinavia, it is also worth noting that the POAM observations show that both 25° to the east of the DLR flight track (40.2°E) and, to a lesser extent, 25° to the west of the flight track (349°E) much larger PSCs were still present on 27 January (extinction ratio peaks of 72 and 15, respectively).

[27] In summary, airborne lidar and balloon measurements made as part of the SOLVE/THESEO 2000 campaign have provided an excellent opportunity to evaluate POAM PSC measurements. We find that the altitude of the large-scale PSC features and morphology are well reproduced in

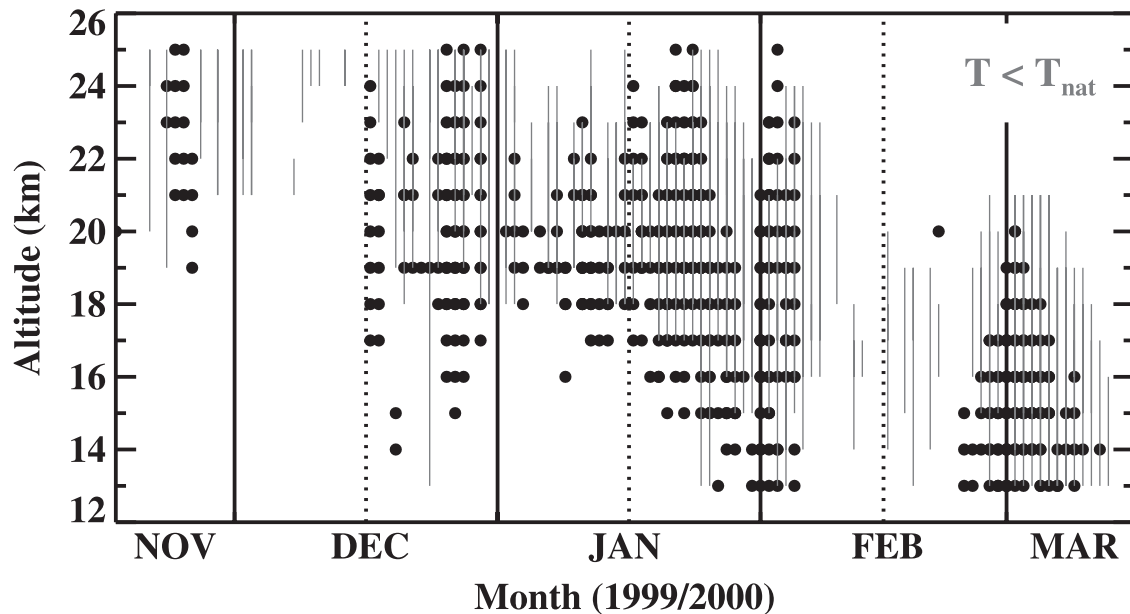


Figure 7. The seasonal evolution of PSCs observed by POAM plotted as a function of altitude and time over the 1999/2000 winter. The dots denote the altitudes and times of all POAM retrieval layers in which a PSC was observed. Vertical lines denote the regions of the atmosphere, for each POAM measurement, which were saturated with respect to NAT (i.e., $T < T_{\text{NAT}}$). In this case the T_{NAT} values were computed using a constant HNO_3 mixing ratio of 10 ppbv, and measured POAM H_2O mixing ratios. The heavy vertical lines denote the beginning of each month, and the dotted lines the midpoint of the month. The POAM PSC detection algorithm search altitude range is 13–25 km.

the POAM measurements. Overall, the comparisons shown here illustrate that POAM measurements (as well as those from similar satellite-based instruments) provide important PSC information, which is useful for PSC composition and morphology studies.

5. Overview of POAM PSC Observations During the 1999/2000 Winter

5.1. PSC Seasonal Evolution

[28] In Figure 7 we show the altitudes and times of all PSCs observed by POAM during the 1999/2000 Northern Hemisphere winter. PSCs were observed between 20 November and 15 March, roughly consistent with the time period in which Figure 2 indicates minimum temperatures were below the NAT saturation temperature at the POAM latitude. In the previous POAM II/III measurement years (1993–1996, and 1998), PSCs in the Northern Hemisphere have been observed as early as mid-November and as late as 3 April. At brief intervals from November through February, the number of PSCs observed in 1999/2000 was as large as at any point in the POAM record, but for most of this period, the 1999/2000 PSCs are not unusually abundant. PSCs are an intermittent phenomenon until mid-December, but they become more frequent (but still with some breaks) into January. From 11 January through 7 February, POAM recorded at least one PSC profile each day. PSCs were absent at the POAM measurement latitude between 8 and 22 February, then returned in the latter part of February. The three-week PSC episode between 23 February and 15 March was the longest period of continuous daily observations of PSCs ever observed by POAM II

or POAM III in March. In fact, POAM observations suggest that PSCs generally become rare this late in the season. Also, *Poole and Pitts* [1994] reported just a few PSC sightings in March in their 12-year SAM II PSC climatology. However, in 1996/1997, an Arctic winter without POAM measurements, the Improved Limb Atmospheric Spectrometer (ILAS) satellite instrument observed PSCs into mid-March [*Hayashida et al.*, 2000].

[29] Most of the PSCs observed by POAM during the 1999/2000 winter were either inside the vortex, or on the vortex edge. However, PSCs were observed outside the vortex on five days: 6 December, 20, 23, 24, and 25 January. In this, as in other POAM years, the PSCs outside the vortex are usually found in conjunction with other PSCs observed at the vortex edge. This can be seen, for example, in the 25 January observations. Figure 3a shows that the PSC observed over the Norwegian Sea on that day (the DIAL coincidence profile) was located near the vortex edge on the 500 K surface. However, the PSC extended down to about the 440 K surface (approximately 19 km) and (because of the vortex vertical tilt) at this level (not shown) was just outside the outer edge of the vortex.

5.2. PSC Composition

[30] POAM observed no ice clouds during the 1999/2000 winter (POAM did observe ice clouds during the 1994/1995, and 1995/1996 Northern Hemisphere winters [*Fromm et al.*, 1999], which were also very cold). This is consistent with Figure 2, which shows that minimum temperatures at the POAM measurement latitude did not fall below the water ice frost point during the 1999/2000 winter. The

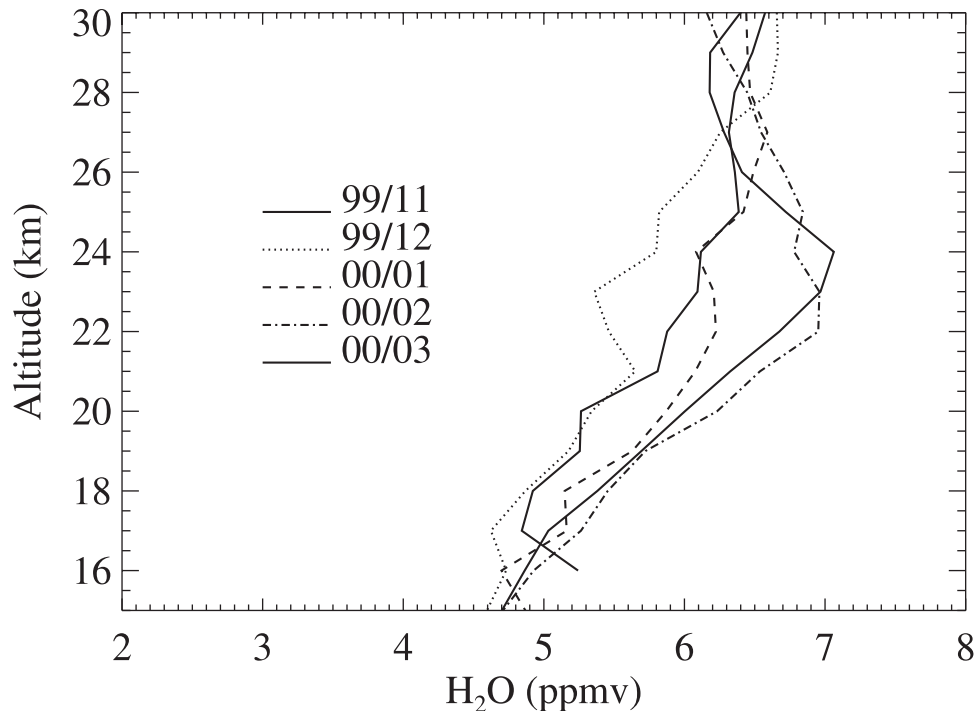


Figure 8. Monthly average Arctic inside vortex POAM III H₂O mixing ratio profiles for the 1999/2000 winter. Monthly averages were computed from PSC-free profiles only (see section 6).

analysis by *Strawa et al.* [2002] suggests that, of the PSCs observed by POAM, the ratio of crystalline to liquid clouds evolved over the winter from a value of 1.6 in November, increasing to a maximum of 2.0 in January, and decreasing thereafter to 0.8 in March.

6. PSC-Temperature Relationships: Inference of Denitrification

[31] The vertical bars in Figure 7 denote the regions of the atmosphere which were saturated with respect to NAT. This suggests a close correspondence between the altitudes and times of POAM PSC observations, and NAT-saturated air. PSCs in the early season generally occur between 17 and 25 km (the top altitude at which the POAM PSC detection algorithm is used). The central altitude of the PSC observations, roughly 21 km, is unchanged between November and late January. At that point, the PSC altitude range (both top and bottom) decreases somewhat, and becomes more variable. The topmost PSC altitudes (up to 25 km) are reestablished around 5 February, soon after which PSCs temporarily vanish at all altitudes. When PSCs reappear in late February and into March, they form at distinctly lower altitudes, centered roughly at 16 km, coincident with the shift downward of the region of the atmosphere saturated with respect to NAT.

[32] We note that the T_{NAT} values used to construct the vertical bars shown in Figure 7 were computed using a fixed HNO₃ profile of 10 ppbv as in Figure 2. However, in this case, we used POAM water vapor measurements in the T_{NAT} computation. POAM water vapor measurements obtained during SOLVE/THESEO 2000 have been compared with in situ ER-2 measurements by *Danilin et al.*

[2002]. The measurements generally agree to within about 10%, with POAM tending to be somewhat high compared to the ER-2 measurements [*Danilin et al.*, 2002]. It is not possible, however, to simply use the measured POAM water vapor mixing ratios for each POAM point because large aerosol enhancements (such as those obtained in PSCs) can produce an artifact in the POAM water vapor retrievals [see *Nedoluha et al.*, 2000]. Thus POAM cannot reliably measure water vapor in the presence of PSCs. Therefore we have computed monthly average POAM water vapor measurements where the averaging included only measurements without PSCs. Also, since the large majority of PSCs are observed in the vortex, the averaging was restricted to measurements inside the vortex middle edge as defined using the *Nash et al.* [1996] objective vortex delineation scheme. The resultant monthly average water vapor mixing ratio profiles are shown in Figure 8. This figure shows that water vapor mixing ratios inside the vortex in the lower stratosphere increase as the winter progresses as the result of diabatic descent. In order to calculate T_{NAT} for each POAM measurement, we simply interpolate the monthly averaged water vapor mixing ratios shown in Figure 8 linearly in time, at each altitude.

[33] Although Figure 7 does show general qualitative agreement between the regions of PSCs and those of sub- T_{NAT} air, there are also several notable differences. From the start of the season until mid-January, there are several observations of PSCs in air warmer than T_{NAT} . A closer inspection of these observations (not shown) indicates that peak PSC extinctions generally occur in air saturated with respect to NAT, but extinction enhancements greater than the PSC threshold sometimes extend 1 or 2 km below (or in some cases above) the region of the atmosphere saturated

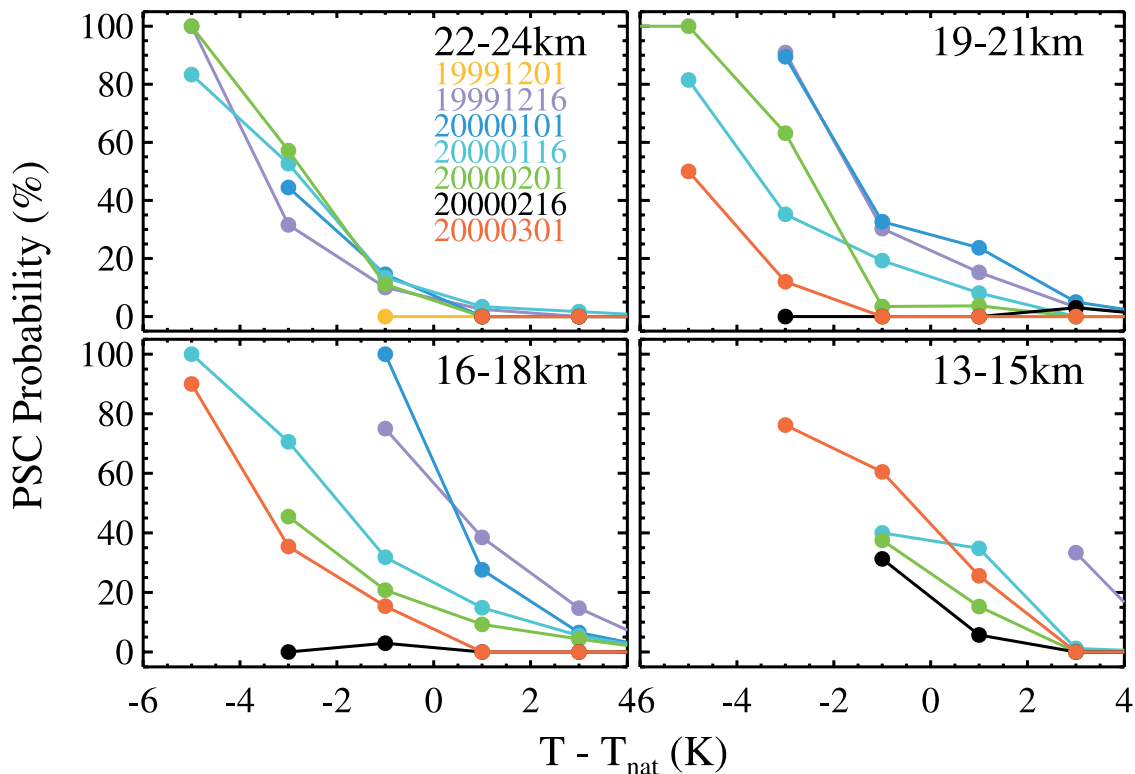


Figure 9. PSC observation probability as a function of $T - T_{\text{NAT}}$ for the indicated altitudes and time periods. For these calculations the data were binned into the indicated 3 km altitude bins, 2 K $T - T_{\text{NAT}}$ bins, and two-week time periods (the beginning of each two-week time period is indicated). The PSC observation probability is defined as the number of PSCs observed in each bin divided by the total number of POAM observations in each bin (expressed in percent).

with respect to NAT. The other noteworthy departure from the correlation between PSCs and temperature is the occurrence of sub- T_{NAT} air in clear sky conditions. This is most apparent in early December, late January at 20–24 km, during the lull in PSC observations in mid-February, and above the PSC observations during the continuously cloudy period from late February to mid-March. We discuss these distinctly cold, clear periods in detail below.

[34] In order to quantify the relationship between PSC occurrence and T_{NAT} suggested in Figure 7, we have computed the POAM PSC observation probability as a function of ambient temperature (relative to T_{NAT}). To calculate the probabilities, the data were binned into 3 km altitude bins, two-week time bins, and 2 K temperature bins. We define the POAM PSC observation probability simply as the number of PSCs observed divided by the number of observations in each time, altitude, and temperature bin. The results are shown in Figure 9. In the 22–24 km bin, in general, we see the expected relationship that as the temperature decreases the probability of PSC occurrence increases. Probabilities approach 100% when the temperatures are lower than T_{NAT} by more than 4 K. Also, other than the earliest period, the curves for all of the two-week periods are roughly similar. However, in the other altitude regions (especially the 19–21 km and 16–18 km regions) there is a distinct evolution of the probabilities as a function of time, with the probabilities generally lower late in the season. This is particularly clear in the 16–29 February time bin

(20000216) in both the 19–21 km and 16–18 km altitude regions.

[35] The 19–21 and 16–18 km regions are particularly interesting because, at these altitudes, there are a sufficient number of observations at temperatures lower than T_{NAT} to compute observation probabilities over a large portion of the winter. Therefore the time evolution of PSC observation probabilities can be examined. In Figure 10, we plot the PSC observation probabilities, at these altitudes, as a function of time for the 2 to 4 K below T_{NAT} temperature bin (hereafter we refer to this simply as the -3 K temperature bin). Here we smooth the probabilities by using a two-week moving average instead of the two-week discrete average shown in Figure 9. Therefore the plotted points, which represent the center of each two-week bin, are not independent. We require at least three measurements in each bin in order to compute a probability. Time periods with fewer than three observations in the -3 K temperature bin are designated by plus signs below the zero line. Also plotted in Figure 10 is the minimum (vortex wide) temperature at 50 hPa. In the 19–21 km altitude region, the major features of the probability variations include the following: probabilities approaching 100% through early January, decreasing rapidly through January, a brief period of increasing probabilities in early February, probabilities approaching 0 in mid-February, and finally a small increase in early March. At 16–18 km, probabilities can be first computed in mid-January when sample sizes become

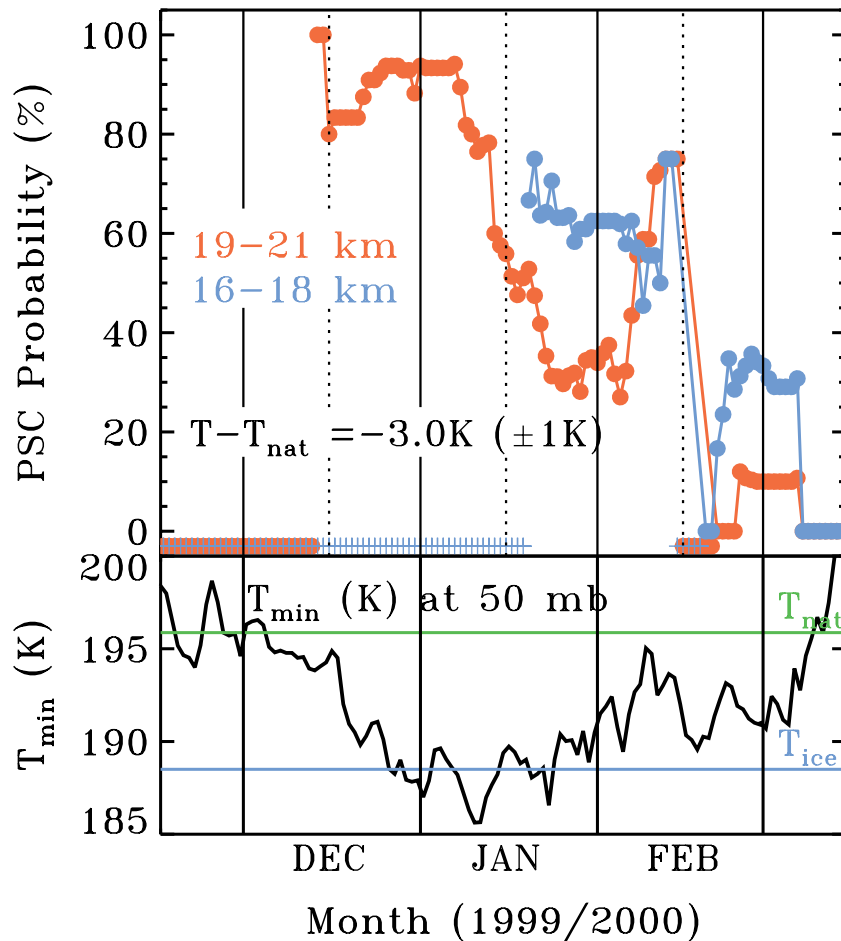


Figure 10. Evolution of PSC observation probability with time for the indicated altitudes. A two-week moving average was used to calculate the probabilities. The center of each two-week period is plotted. In each bin, we require three measurements to compute a probability. Bins containing fewer than three measurements are denoted by plus signs below the zero line. Also shown are vortex-wide minimum temperatures at 50 hPa and the ice and NAT saturation temperatures.

sufficiently large. The variations are generally similar to those observed at 19–21 km, but the increase in early February is sharper, and the increase in late February–early March is somewhat larger.

[36] In order to examine more closely the data upon which the PSC statistics are based, in Figures 11a and 11b we plot the POAM 1018 nm aerosol extinction as a function of ambient temperature, again with respect to the T_{NAT} value, for the indicated time periods for both the 19–21 (Figure 11a) and 16–18 km (Figure 11b) altitude regions. In all panels, the shaded region denotes the -3 K temperature bin used in the probability computations illustrated in Figure 10. These time periods were selected because they are representative of the large-scale variations seen in the evolution of PSC observation probability as a function of time seen in Figure 10. This shows that the increase in the PSC observation probabilities in early February is caused by a PSC episode occurring in the February 6–7 period. As is clear from Figure 7, PSCs briefly reappeared at the higher altitudes during this time after an absence of a few days.

[37] In order to evaluate the statistical significance of the PSC observation probability variations, we use as a reference the 15–30 January time period because it has the

largest number of observations and, therefore, the highest statistical confidence. We estimate the statistical significance of the differences in the PSC observation probability in other time periods compared to the 15–30 January time period by assuming that these probabilities follow a binomial distribution. In this case, the standard deviation of the PSC observation probability in any time bin is simply given by *Bevington and Robinson* [1992]

$$\sigma = (Np(1-p))^{1/2}/N \quad (1)$$

where N is the number of observations in each time bin, and p is the PSC observation probability in the 15–30 January time bin. The probability uncertainties given in Figure 11 have been computed using equation (1) for observations in the -3 K temperature bin. This indicates that the PSC probability variations over the time periods shown in Figure 11 are generally significant at least at the 1σ level. The exceptions include the PSC observation probability difference between the 15–31 January and 6–7 February periods, which are right at the 1σ level. However, the fact that we see the same tendency in both altitude bins increases confidence in the

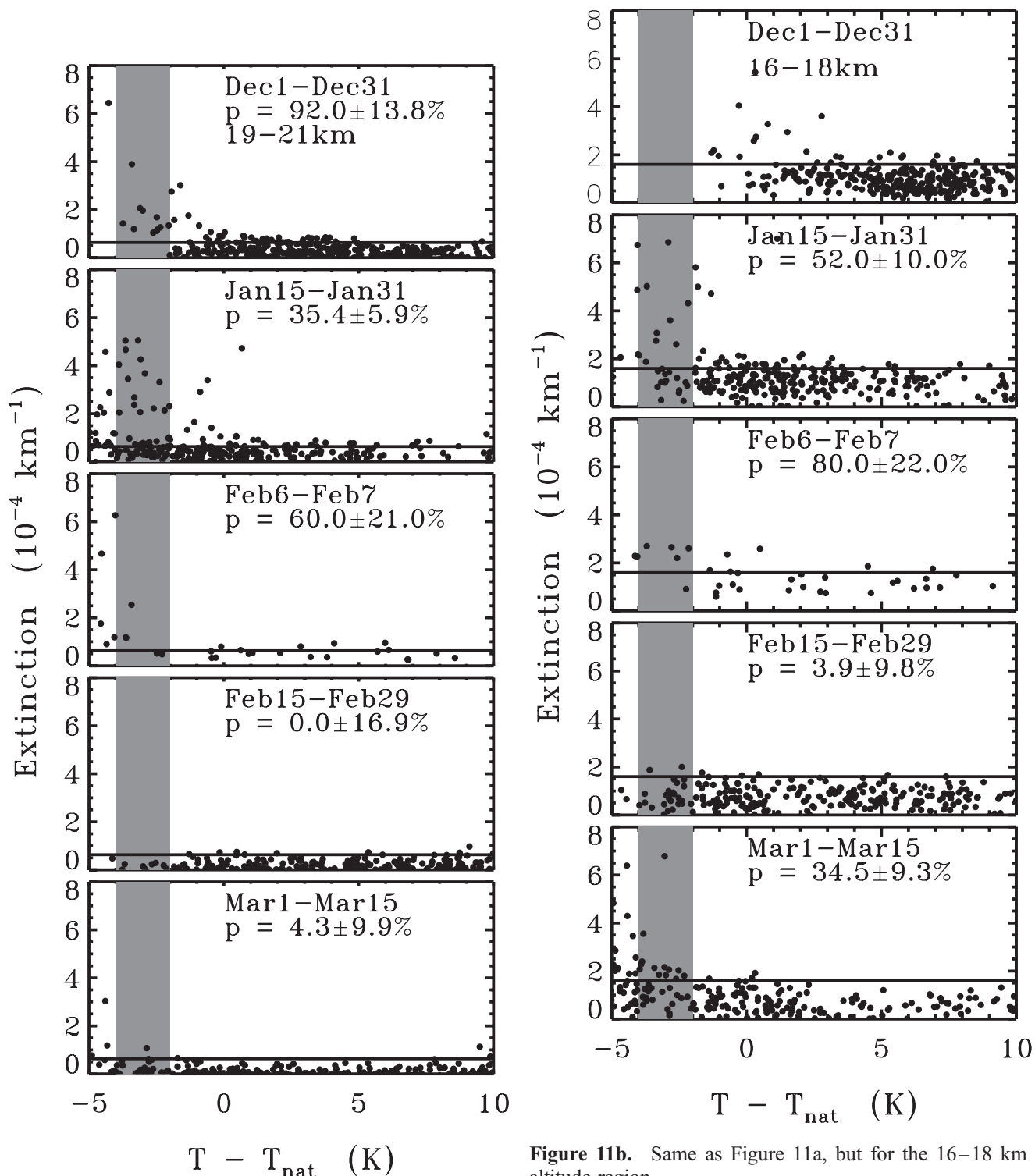


Figure 11a. Aerosol extinction at 1018 nm plotted as a function of $T - T_{\text{NAT}}$ for the indicated time periods in the 19–21 km altitude range. The horizontal lines are the PSC threshold values at the midpoint of each altitude range. The shaded region denotes the -3 K temperature region used in the probability computations illustrated in Figure 10. The PSC occurrence probability in the -3 K temperature region (p), and associated uncertainty, is shown on each panel.

Figure 11b. Same as Figure 11a, but for the 16–18 km altitude region.

statistical significance of the variation. Also, the difference between the PSC observation probability in the February 15–29 time period compared with that obtained in the 1–15 March time period in the 19–21 km altitude bin is not statistically significant at the 1σ level. However, in the 16–18 km altitude region the probability difference over the same two time periods is significant.

[38] Having generally established the statistical significance of the PSC observation probability variations shown

in Figure 10, the next step is to investigate their origin. We have identified the following possible mechanisms: time-varying systematic temperature errors or biases, variations in PSC composition (and thus also PSC formation temperatures), dehydration, and denitrification. In the following we discuss each of these possible mechanisms in turn, and conclude that the extensive denitrification which was observed during the 1999/2000 winter [Popp *et al.*, 2001] is the most likely cause of the POAM PSC observation probability variations.

[39] Time-varying systematic biases in the UKMO temperature analysis would produce PSC observation probability variations. In fact, given the sensitivity of PSC activation to temperature, these biases need not be very large. For example, if the UKMO temperatures at 20 km were biased lower in December and early February compared to late January by 2 K, then the observation probabilities for these periods would be similar. The presence of time-varying biases in the UKMO analysis, and their importance in the PSC observation probability variations, is exceedingly difficult to identify because of the scarcity of temperature measurements encompassing the entire winter. However, minimum vortex temperatures at 46 hPa for the 1999/2000 winter obtained from the US National Center for Environmental Prediction (NCEP) and UKMO analyses (the NCEP analysis tends to be more closely tied to the sondes in the lower stratosphere) (R. Swinbank, personal communication, 2001) have been compared by Manney and Sabutis [2000]. They do find time-varying systematic differences between the two analyses, with UKMO tending to be colder than NCEP by 1–3 K in the mid-December through mid-January period, and again in late February [Manney and Sabutis, 2000]. However, the time-varying biases (even if one attributes them totally to UKMO errors) cannot completely explain the PSC observation probability evolution depicted in Figures 10 and 11. For example, accounting for these variations in this way would require a maximum UKMO cold bias in late February, and an increasing cold bias during the latter part of January. Such biases are not seen in the analysis by Manney and Sabutis [2000].

[40] In order to investigate possible temperature biases further, we have compared temperature profiles obtained from electrochemical concentration cell (ECC) sondes launched at Orland (63.42°N), Salekhard (66.7°N), and Sodankyla (67.4°N) in the early part of the winter with the UKMO analysis interpolated to the time and location of the ECC sonde launches. These particular ECC sonde stations were chosen because they are all close to the POAM measurement latitudes. Taken together, the 13 soundings from Orland, the 10 soundings from Salekhard, and the 21 soundings from Sodankyla cover the period from 3 November 1999 through 1 February 2000. It is important to point out that, because the UKMO analysis does assimilate ECC sonde temperatures, this is not a completely independent comparison. However, since the UKMO analysis is much more heavily weighted to satellite data than to individual sonde measurements (R. Swinbank, personal communication, 2001), the comparison is meaningful. We do find large differences between the sondes and the UKMO analysis in individual comparisons (approaching 4 K). However, although individual differences tend to be larger later in the season, no clear time-varying systematic

biases emerge which are consistent in the comparisons at all three sites. The mean bias ($T(\text{sonde}) - T(\text{UKMO})$), combining all three sites over the entire time period, is 0.33 ± 0.25 K (1-sigma). Thus although it is not possible to completely rule out time-varying systematic temperature errors, the available evidence suggests that such errors cannot completely explain the PSC observation probability variations seen in Figures 10 and 11.

[41] The formation temperature of STS (supercooled ternary solution) PSCs (type Ib) is approximately 4 K lower than that of NAT clouds [Tabazadeh *et al.*, 1994]. Thus a variation with time in the occurrence of NAT relative to that of STS PSCs would be expected to cause variations in the overall POAM PSC observation probability at a given temperature. As mentioned previously, Strawa *et al.* [2002] have used the POAM aerosol extinction and extinction color ratio to distinguish NAT from STS clouds. This analysis does indicate an overall decrease in the NAT to STS occurrence fraction from late January through the end of the winter, which would be expected to result in a decrease in the PSC observation probability, at a given temperature, over that time period. This is qualitatively consistent with the time evolution of the PSC observation probability seen in Figure 10. However, the details of the time evolution over the entire winter are not consistent. For example, the NAT/STS occurrence fraction is seen to peak in mid to late January, with values somewhat larger than those obtained in December. However, the PSC observation probability at -3 K decreases by about a factor of 2 over this time period. Similarly, the NAT/STS fraction decreases from late January into early February, while the PSC observation probability increases. Thus we conclude that, although there were time-varying systematic variations in the NAT/STS occurrence fraction during the 1999/2000 winter, these variations do not appear to be well correlated with the observed variations in the PSC occurrence probabilities.

[42] The NAT saturation temperature is a strong function of the water vapor mixing ratio. As explained above, in the NAT computation, we use POAM monthly averaged water vapor mixing ratios obtained from measurements inside the vortex in cloud-free air (see Figure 8). This accounts for the long-term water vapor variations, which are mainly the result of diabatic descent. However, local dehydration of parcels of air containing PSCs would not be seen in the POAM monthly averaged measurements. Nedoluha *et al.* [2002], have performed a much more extensive analysis of the POAM water vapor measurements and find no significant dehydration during the 1999/2000 Northern Hemisphere winter. In situ NASA ER-2 measurements and balloon-borne measurements [Schiller *et al.*, 2002], obtained as part of the SOLVE/THESEO 2000 campaign, do find evidence for a small amount of irreversible dehydration (0.5 ppmv). However, this is not large enough to impact significantly the POAM PSC observation probability variations.

[43] Poole and Pitts [1994] have noted PSC occurrence probability variations in Stratospheric Aerosol Measurement (SAM II) measurements in the Antarctic, and linked them to denitrification. The idea is that HNO_3 depletion lowers the NAT saturation temperature, and thus the temperature required for PSC formation. This results in lower PSC

observation probabilities at a given temperature. Extensive denitrification was observed in the 1999/2000 winter, as part of the SOLVE/THESEO 2000 mission, in airplane-based and balloon-borne measurements [Popp *et al.*, 2001]. In addition, in March the denitrification was sufficiently widespread to be observed in Microwave Limb Sounder (MLS) satellite measurements [Santee *et al.*, 2000]. It is likely that the PSC occurrence probability variations shown in Figures 10 and 11 contain the signature of this denitrification. However, it is important to note that these probability variations would only be sensitive to irreversible denitrification, and not to temporary sequestration of HNO_3 in PSC particles. This is true simply because the technique is based on finding statistically significant decreases in the number of measurements at a given temperature which are cloud free. Within the denitrification scenario, this can only happen when HNO_3 is permanently removed from the parcel. Also, since we have used a constant HNO_3 mixing ratio to calculate T_{NAT} in the probability calculations, relative variations are important, but absolute probability values have little significance.

[44] If we interpret the PSC probability time variations shown in Figure 10 in terms of denitrification, the following scenario evolves. At 19–21 km, significant denitrification is first inferred at the beginning of January, roughly coincident with the time that the minimum vortex temperature at 50 hPa (shown in Figure 10) decreases to the frost point. Denitrification maximizes at the end of February. At 16–18 km, the rate of denitrification in the latter half of January is not as large as at 19–21 km. The denitrification at 16–18 km also peaks in late February. However, the recovery in early March is larger than at 19–21 km. The increase in the probabilities in early February at both 16–18 and 19–21 km, which is marginally significant, is much more difficult to interpret in terms of the denitrification scenario. This is because the POAM water vapor and ozone measurements (not shown) show no evidence of intravortex mixing or enhanced (relative to that obtained normally in the vortex) diabatic descent during this period. This implies that there is no mechanism for renitrification of the atmosphere over the required timescales. However, we do find that the PSCs observed by POAM in that early February period did tend to occur deeper in the vortex (higher equivalent latitude) than those observed immediately before in late January. Thus we believe that the increase in the observation probability in early February is much more likely to have resulted from spatial inhomogeneities in the HNO_3 field and POAM sampling differences, than renitrification of the atmosphere.

[45] It is difficult to make quantitative estimates regarding the amount of denitrification from the PSC probability variations because it is not possible to separate the effect of random temperature error from inhomogeneities in the HNO_3 mixing ratio of parcels sampled by POAM. However, we do note that the NAT saturation temperature is a fairly weak function of the HNO_3 mixing ratio. Very roughly, at lower stratospheric pressures and typical HNO_3 mixing ratios, a 50% HNO_3 mixing ratio decrease produces a 1 K decrease in the saturation temperature. Figure 11 shows that in December at 19–21 km all observations in the -3 K temperature bin were PSCs, while in late February none were PSCs. This suggests that the PSC formation temperature was at least 2 K higher in

December than in late February. With the relationship between T_{NAT} and HNO_3 mixing ratio given above, this would imply that the HNO_3 mixing ratio of all air parcels sampled by POAM in this altitude range was reduced by at least 75% compared to their December values. The probabilities suggest that the denitrification at 16–18 km was about equally as deep in late February, but the recovery is more rapid in early March. No denitrification was inferred above 21 km. Finally, we note that the relatively high PSC observation probabilities seen in Figure 9 at 13–15 km for $T > T_{\text{NAT}}$, especially during January where it reaches 40% in the 0 to +2 K bin, suggest that the HNO_3 mixing ratio might exceed the 10 ppbv value, which we assume in the T_{NAT} calculation. This could indicate that some of the HNO_3 that was sequestered in the PSCs at higher altitudes was released once the clouds fell to altitudes where the temperatures were above T_{NAT} , enhancing the HNO_3 amounts at these lower altitudes, and allowing the increased probability of PSC formation at warmer temperatures.

[46] The degree of denitrification inferred from the POAM data is large compared to the roughly 20% denitrification detected by MLS at the end of the 1999/2000 winter reported by Santee *et al.* [2000]. However, as pointed out in that study, the MLS measurements do not preclude much larger denitrification on smaller vertical scales than those detectable by MLS. This is relevant because the POAM measurements have finer vertical resolution than the MLS measurements (POAM: 1–2 km, MLS: 4–6 km). Furthermore, the MLS measurements from which denitrification was inferred were made in late March; it is possible that some renitrification had occurred by that time. In fact, the POAM measurements suggest that a significant renitrification may have occurred by mid-March (see Figures 10 and 11) in the 16–18 km region.

[47] In situ ER-2 measurements during SOLVE/THESEO 2000 show denitrification of $>60\%$ inside the vortex at equivalent latitudes between 70° and 85°N , with local values of $>80\%$; denitrification was observed to maximize in the 20–21 km region (maximum ER-2 altitude), and no denitrification was observed below 16 km [Popp *et al.*, 2001]. Thus the denitrification inferred from the POAM PSC observation probability variations is consistent, both in terms of magnitude and altitude extent, with that observed by the ER-2.

[48] While a large degree of denitrification was observed during the 1999/2000 winter, as mentioned previously, only a small amount of dehydration was observed. This implies that NAT (or nitric acid dihydrate, NAD) clouds were the primary denitrifying agent during this winter, since STS clouds are unlikely to grow to large enough sizes to have sufficient fall speeds to effectively denitrify the atmosphere [Tabazadeh *et al.*, 2000]. In fact, NAT particles with radii as large as 10–20 μm (large enough to denitrify the atmosphere) were observed between January and March 2000 by in situ ER-2 measurements [Fahey *et al.*, 2001]. NAT clouds were also shown to cause significant denitrification in the early part of the Antarctic winter (before temperatures reach the frost point) by Tabazadeh *et al.* [2000]. The general features of the denitrification inferred from the POAM data in the 1999/2000 winter (maximum rate of denitrification in January, and minimum values in late February-early March) are broadly consistent with the temperature evolution over

the winter. Figure 10 shows that the coldest vortex temperatures occurred in January, where minimum temperatures were generally near or less than the frost point. Lower temperatures imply larger exposure times below T_{NAT} and, therefore, more opportunities for the formation of NAT clouds. Several studies [e.g., Tabazadeh *et al.*, 1996; Larsen *et al.*, 1996, 1997; Santee *et al.*, 2002] have concluded that NAT (or NAD) clouds form from STS clouds only after exposure to sub- T_{NAT} temperatures for more than 1 day. In early March, minimum vortex temperatures increased rapidly to values well above T_{NAT} by mid-March. The enhanced dynamical activity resulting in the final warming could have acted to initiate the renitrification of the atmosphere at this time both by enhanced descent and mixing, resulting in the increase in the PSC observation probabilities seen in Figure 10.

7. Summary and Conclusions

[49] We have presented an overview of PSC measurements obtained by POAM in the 1999/2000 Northern Hemisphere winter. PSCs were observed between 20 November and 15 March. PSCs in the early season generally occurred between 17 and 25 km (the highest altitude used in the PSC detection algorithm). The central altitude of the PSC observations, roughly 21 km, is unchanged between November and late January. PSCs were not observed at the POAM measurement latitudes between 7 and 27 February. When they reappeared they formed at distinctly lower altitudes, centered roughly at 16 km.

[50] We have also compared the POAM PSC measurements to other measurements made as part of the SOLVE/THESEO 2000 campaign during the 25–27 January 2000 period. During this period there was a direct measurement coincidence with the DIAL instrument on board the DC-8, and the OLEX instrument on board the DLR Falcon. In both cases the agreement between POAM and the lidar measurements was good in terms of PSC vertical extent and composition. In addition to the two quantitative comparisons, we have shown that the general morphology of PSCs over Scandinavia from 25 to 27 January, as revealed by the airplane and balloon-borne measurements, is well produced in the POAM measurements. When viewed together, the measurements suggest that the mountain wave activity, which was well documented during this period by the airborne lidar measurements [Dörnbrack *et al.*, 2002], acted to enhance and perturb an existing synoptic-scale PSC feature.

[51] Finally, we have investigated the evolution of the PSC occurrence probability as a function of ambient temperature (relative to T_{NAT}) during the 1999/2000 winter. We find statistically significant changes in these occurrence probabilities over the winter. We conclude that these probability variations are most probably the manifestation of irreversible denitrification. This denitrification is first apparent in early January, and maximizes in the late February-early March time period. We infer that by the end of February the denitrification reached levels of at least 75% in the 19–21 km region. The denitrification was about the same at 16–18 km, but recovered more rapidly in early March. Denitrification was significantly smaller at 13–15 km, and no denitrification was inferred above 21 km.

[52] **Acknowledgments.** We thank the NASA Goddard Space Flight Center for supplying the UKMO analyses. We acknowledge helpful conversations with G. Manney. This research was supported by the Office of Naval Research and by NASA under the Scientific Data Purchase Program and Upper Atmospheric Research Program.

References

- Appenzeller, C., H. C. Davies, and W. A. Norton, Fragmentation of stratospheric intrusions, *J. Geophys. Res.*, *101*, 1435–1456, 1996.
- Bevington, P. R., and D. K. Robinson, *Data Reduction and Error Analysis for the Physical Sciences*, McGraw-Hill, New York, 1992.
- Butchart, N., and E. E. Remsburg, The area of the stratospheric polar vortex as a diagnostic for tracer transport on an isentropic surface, *J. Atmos. Sci.*, *43*, 1319–1339, 1986.
- Danilin, M. Y., et al., Comparison of the aircraft ER-2 and satellite POAM-III, MLS, and SAGE-II measurements during SOLVE using traditional correlative analysis and trajectory hunting technique, *J. Geophys. Res.*, *107*, 10.1029/2001JD000781, in press, 2002.
- Dörnbrack, A., T. Birner, A. Fix, H. Flentje, A. Meister, H. Schmid, E. V. Browell, and M. J. Mahoney, Evidence for inertia-gravity waves forming polar stratospheric clouds over Scandinavia, *J. Geophys. Res.*, *107*, 10.1029/2001JD000452, in press, 2002.
- Fahey, D. W., et al., The detection of large HNO_3 -containing particles in the winter Arctic stratosphere, *Science*, *291*, 1026–1031, 2001.
- Fromm, M. D., et al., Observations of Antarctic polar stratospheric clouds by POAM II: 1994–1996, *J. Geophys. Res.*, *102*, 23,659–23,672, 1997.
- Fromm, M. D., et al., An analysis of POAM II Arctic polar stratospheric cloud observations, 1993–1996, *J. Geophys. Res.*, *104*, 24,341–24,357, 1999.
- Glaccum, W., et al., The Polar Ozone and Aerosol Measurement (POAM II) instrument, *J. Geophys. Res.*, *101*, 14,479–14,487, 1996.
- Hanson, D., and K. Mauersberger, Laboratory studies of the nitric acid trihydrate: Implications for the south polar stratosphere, *Geophys. Res. Lett.*, *15*, 855–858, 1988.
- Hayashida, S., N. Saitoh, A. Kagawa, T. Yokota, M. Suzuki, H. Nakajima, and Y. Sasano, Arctic polar stratospheric clouds observed with the Improved Limb Atmospheric Sounder during winter 1996/1997, *J. Geophys. Res.*, *105*, 24,715–24,730, 2000.
- Jansco, G., J. Pupezin, and W. A. Hook, The vapor pressure over ice between $+10^{-2}$ and -10^{+20} , *J. Phys. Chem.*, *74*, 2984–2989, 1970.
- Larsen, N. B., B. M. Knudsen, J. M. Rosen, N. T. Kjöme, and E. Kyrö, Balloonborne backscatter observations of type 1 PSC formation: Inference about physical state from trajectory analysis, *Geophys. Res. Lett.*, *23*, 1091–1094, 1996.
- Larsen, N. B., B. M. Knudsen, J. M. Rosen, N. T. Kjöme, R. Neuber, and E. Kyrö, Temperature histories in liquid and solid polar stratospheric cloud formation, *J. Geophys. Res.*, *102*, 23,505–23,517, 1997.
- Lucke, R. L., et al., The Polar Ozone and Aerosol Measurement (POAM) III instrument and early validation results, *J. Geophys. Res.*, *104*, 18,785–18,799, 1999.
- Lumpe, J. D., et al., Comparison of POAM III ozone measurements with correlative aircraft and balloon data during SOLVE, *J. Geophys. Res.*, *107*, doi:10.1029/2001JD000472, in press, 2002a.
- Lumpe, J. D., R. Bevilacqua, K. W. Hoppel, and C. E. Randall, POAM III retrieval algorithm and error analysis, *J. Geophys. Res.*, doi:10.1029/2002JD002137, in press, 2002.
- Manney, G. L., and J. L. Sabutis, Development of the polar vortex in the 1999–2000 Arctic winter stratosphere, *Geophys. Res. Lett.*, *27*, 2589–2592, 2000.
- Manney, G. L., W. A. Lahoz, R. Swinbank, A. O'Neill, P. M. Connery, and R. W. Zurek, Simulation of the December 1998 stratospheric major warming, *Geophys. Res. Lett.*, *26*, 2733–2736, 1999.
- Mauldin, L. E., III, N. H. Zaun, M. P. McCormick, J. H. Guy, and W. R. Vaughn, Stratospheric Aerosol and Gas Experiment II Instrument: A functional description, *Opt. Eng.*, *24*, 307–312, 1985.
- Nash, E. R., P. A. Newman, J. E. Rosenfield, and M. R. Schoeberl, An objective determination of the polar vortex using Ertel's potential vorticity, *J. Geophys. Res.*, *101*, 9471–9478, 1996.
- Nedoluha, G. E., R. M. Bevilacqua, K. W. Hoppel, M. Daehler, E. P. Shettle, J. S. Hornstein, M. D. Fromm, J. D. Lumpe, and J. E. Rosenfield, POAM III measurements of dehydration in the Antarctic lower stratosphere, *Geophys. Res. Lett.*, *27*, 1683–1686, 2000.
- Nedoluha, G. E., R. M. Bevilacqua, and K. W. Hoppel, POAM III measurements of dehydration in the Antarctic and comparisons with the Arctic, *J. Geophys. Res.*, *107*, 10.1029/2001JD001184, in press, 2002.
- Pawson, S., and B. Naujokat, The cold winters of the middle 1990s in the northern lower stratosphere, *J. Geophys. Res.*, *104*, 14,209–14,222, 1999.

- Poole, L. R., and M. C. Pitts, Polar stratospheric cloud climatology based on Stratospheric Aerosol Measurement II observations from 1978 to 1989, *J. Geophys. Res.*, *99*, 13,083–13,089, 1994.
- Popp, P. J., et al., Severe and extensive denitrification in the 1999–2000 Arctic winter stratosphere, *Geophys. Res. Lett.*, *28*, 2875–2878, 2001.
- Randall, C. E., R. M. Bevilacqua, J. D. Lumpe, and K. W. Hoppel, Validation of POAM III aerosols: Comparison to SAGE II and HALOE, *J. Geophys. Res.*, *106*, 27,525–27,536, 2001.
- Russell, J. M., III, L. L. Gordley, J. H. Park, S. R. Drayson, W. D. Hesketh, R. J. Cicerone, A. F. Tuck, J. E. Frederick, J. E. Harries, and P. J. Crutzen, The Halogen Occultation Experiment, *J. Geophys. Res.*, *98*, 10,777–10,797, 1993.
- Santee, M. L., G. L. Manney, N. J. Livesey, and J. W. Waters, UARS Microwave Limb Sounder observations of denitrification and ozone loss in the 2000 Arctic late winter, *Geophys. Res. Lett.*, *27*, 3213–3216, 2000.
- Santee, M. L., A. Tabazadeh, G. L. Manney, M. D. Fromm, R. M. Bevilacqua, J. W. Waters, and E. J. Jensen, A Lagrangian approach to inferring the composition of arctic polar stratospheric clouds from UARS MLS HNO₃ and POAM II aerosol extinction measurements, *J. Geophys. Res.*, *107*, 10.1029/2000JD000227, 2002.
- Schiller, C., et al., Dehydration in the Arctic stratosphere during the THESEQ2000/SOLVE campaigns, *J. Geophys. Res.*, *107*, 10.1029/2001JD000463, in press, 2002.
- Solomon, S., Stratospheric ozone depletion: A review of concepts and history, *Rev. Geophys.*, *37*, 275–316, 1999.
- Strawa, A. W., K. Drdla, M. Fromm, P. F. Poeschel, K. W. Hoppel, E. V. Browell, C. A. Hostetler, and P. Hamill, Discriminating type Ia and Ib polar stratospheric clouds in POAM satellite data, *J. Geophys. Res.*, *107*, 10.1029/2001JD000458, in press, 2002.
- Swinbank, R., and A. O'Neill, A stratosphere-troposphere data assimilation system, *Mon. Weather Rev.*, *122*, 686–702, 1994.
- Tabazadeh, A., R. P. Turco, K. Drdla, M. Z. Jacobson, and O. B. Toon, A study of type I polar stratospheric cloud formation, *Geophys. Res. Lett.*, *21*, 1619–1622, 1994.
- Tabazadeh, A., O. B. Toon, B. L. Gary, J. T. Bacmeister, and M. R. Schoeberl, Observational constraints on the formation of type Ia polar stratospheric clouds, *Geophys. Res. Lett.*, *23*, 2109–2112, 1996.
- Tabazadeh, A., M. L. Santee, M. Y. Danilin, H. C. Pumphrey, P. A. Newman, P. J. Hamill, and J. L. Mergenthaler, Quantifying denitrification and its effects on ozone recovery, *Science*, *268*, 1407–1411, 2000.
- Voigt, C., et al., Nitric acid trihydrate (NAT) in polar stratospheric clouds, *Science*, *290*, 1756–1758, 2000.
-
- J. M. Alfred, M. D. Fromm, and J. D. Lumpe, Computational Physics, Inc., 8001 Braddock Road, Suite 210, Springfield, VA 22151, USA. (alfred@cpi.com; fromm@nrl.navy.mil; lumpe@cpi.com)
- R. M. Bevilacqua, K. W. Hoppel, J. S. Hornstein, G. E. Nedoluha, and E. P. Shettle, Naval Research Laboratory, Code 7220, Washington, D.C. 20375, USA. (bevilacqua@nrl.navy.mil; karl.hoppel@nrl.navy.mil; hornstein@nrl.navy.mil; nedoluha@nrl.navy.mil; shettle@nrl.navy.mil)
- E. V. Browell, Lidar Application Group, NASA Langley Research Center, Mail Stop 401A, Hampton, VA 23681, USA. (e.v.browell@larc.nasa.gov)
- A. Dörnbrack, DLR Oberpfaffenhofen, Institut für Physik der Atmosphäre, D-82230 Wessling, Germany. (andreas.dornbrack@dlr.de)
- C. E. Randall, Laboratory for Atmospheric and Space Physics, Campus Box 392, University of Colorado, Boulder, CO 80309-0392, USA. (randall@lasp.colorado.edu)
- W. Strawa, NASA Ames Research Center, Moffett Field, CA, USA. (Strawa:astrawa@mail.arc.nasa.gov)